

The Hubble Deep Field and the Disappearing Dwarf Galaxies

HENRY C. FERGUSON

Space Telescope Science Institute, 3700 San Martin Drive
Baltimore, MD 21218
email: ferguson@stsci.edu

ARIF BABUL

Department of Physics & Astronomy
University of Victoria
3800 Finnerty Road, Victoria, BC V8W 3P6
email: babul@alMuhit.phys.uvic.ca

ABSTRACT

Several independent lines of reasoning, both theoretical and observational, suggest that the very faint ($B \gtrsim 24$) galaxies seen in deep images of the sky are small low-mass galaxies that experienced a short epoch of star formation at redshifts $0.5 \lesssim z \lesssim 1$ and have since faded into low luminosity, low surface brightness objects. Such a scenario, which arises naturally if star formation in dwarf galaxies is delayed by photoionisation due to the metagalactic UV radiation field, provides an attractive way to reconcile the Einstein-de Sitter ($\Omega = 1; \Lambda = 0$) cosmological model to the steeply rising galaxy counts observed at blue wavelengths. Babul and Ferguson (1996) constructed a specific realisation of this model, deriving the dwarf galaxy mass function from the CDM power spectrum, and arguing that the gas in these halos will recombine at $z \sim 1$. The Hubble Deep Field (HDF) images provide a stringent test of this model. We compare the model to the data by constructing simulated images that reproduce the spatial resolution and noise properties of the real data and carrying out source detection and photometry for the simulations in the same way they were carried out for the real data. The selection biases and systematic errors that are inevitable in dealing with faint galaxies are thus incorporated directly into the model. We compare the model predictions for the counts, sizes, and colours of galaxies observed in the HDF, and to the predictions from a low q_0 pure-luminosity-evolution (PLE) model. Both models fail to reproduce the observations. The low q_0 model predicts far more Lyman-break “dropouts” than are seen in the data. The fading dwarf model predicts too many remnants: faded dwarf galaxies in the redshift range $0.2 < z < 0.5$ that should be detectable

in the HDF as low-surface brightness red objects but are not seen. *If fading dwarf galaxies are to reconcile the Einstein-de Sitter geometry to the counts, then the dwarf population must (a) form earlier than $z \sim 1$, with a higher initial luminosity; (b) have an initial-mass function more heavily weighted toward massive stars than the Salpeter IMF; or (c) expand much more than assumed during the supernova wind phase.*

Subject headings: galaxies: formation — galaxies:luminosity function, mass function — galaxies:photometry

1. Introduction

Any self-consistent theory of galaxy evolution and cosmology must now pass the test of matching the distribution of galaxy properties in the Hubble Deep Field. The theory must simultaneously match the counts, redshift and colour distributions, clustering properties, and size distribution of faint galaxies. Even at ground-based depths (e.g. Lilly et al. 1995; Ellis et al. 1996; Cowie et al. 1996), matching the observed distributions within an Einstein-de Sitter ($\Omega = 1$, $\Lambda = 0$) cosmology has required either introducing heuristic modifications to the local luminosity function and the evolution of low-mass galaxies (Phillipps & Driver 1995), or introducing additional physical processes into theories of galaxy evolution beyond simple passive evolution of the stellar populations. In hierarchical prescriptions (e.g. Kauffmann, Guiderdoni, & White 1994; Cole et al. 1994) the additional physics has been a detailed treatment of the merging histories of galaxies, coupled with prescriptions for how star formation proceeds during the merger events. The primary physical process driving the counts in these models is triggered star formation. An alternative view (Babul & Rees 1992; Babul & Ferguson 1996) is that the important physics driving the counts at very faint magnitudes is the delayed formation of dwarf galaxies, where the cooling and collapse timescales of the interstellar gas is governed by photoionisation by the UV background.

The purpose of this paper is to test this latter model against the Hubble Deep Field (HDF) observations. The comparison involves constructing simulated HDF images from Monte-Carlo realisations of the underlying model and then analyzing them in exactly the same manner as the actual images. In this way all of the details of galaxy selection and photometry are properly taken into account.

It is illustrative to consider the $q_0 = 0.5$ dwarf-dominated model not in isolation, but in comparison to a low- Ω giant-dominated model. Gronwall & Koo (1995) and

Pozzetti, Bruzual, & Zamorani (1996) have demonstrated that *for low values of q_0* straightforward “pure-luminosity evolution” models, without large populations of dwarf galaxies or substantial number-evolution, can be reasonably successful at matching the observed counts and redshift distributions (to 1995 ground-based limits). Thus, as a foil to the dwarf-dominated $q_0 = 0.5$ model, we construct a giant-dominated $q_0 = 0.01$ model and carry out the same comparisons to the observations.

We emphasize that our goal in this paper is not to tune the models to try to match the observations, but to test the models in their simplest form to illustrate their differences (and their deficiencies) at the depths probed by the Hubble Deep Field. The models incorporate the simplest, most conservative, assumptions for the luminosity function of local giant galaxies, their stellar initial mass functions and evolution, their star-formation histories, and their surface-brightness distributions. The predictions of both models turn out to be very sensitive to the redshift of formation, which has not been tuned *post-facto* to try to meet the constraints imposed by the observations. The dwarf galaxies are incorporated into the $q_0 = 0.5$ model with only three free parameters (described in section 1). These parameters were fixed from physical arguments and ground-based observations (Babul & Ferguson 1996) and have *not* been tuned to match the HDF observations.

In §2, we briefly review the $q_0 = 0.5$ dwarf-dominated model and the $q_0 = 0.01$ model, and discuss the construction of simulated HDF images from the corresponding Monte-Carlo realisations. In §3, we compare the results for the two models to the observations. In §4 we outline the implications of these comparisons, specifically identifying changes that might be made to each model to bring it more into agreement.

2. The Models

2.1. The $q_0 = 0.5$, bursting-dwarf model

In a $q_0 = 0.5$ cosmology, matching the galaxy number counts and redshift distributions observed to ground-based limits requires a large population of low-luminosity galaxies at moderate redshifts. Babul & Ferguson (1996) outlined a dwarf-dominated model that appeared capable of reproducing existing ground based observations. The model consists of “giant” galaxies (types E through Sdm) that form at $z_f = 5$ and a large population of dwarf galaxies that begin forming stars at $z \approx 1$. (Babul & Ferguson refer to these objects as “boojums,” for blue objects observed just undergoing a moderate starburst). The comoving number density of each galaxy type is conserved, but the dwarfs are entirely gaseous until $z < 1$.

In hierarchical clustering scenarios with realistic initial conditions on galactic and sub-galactic scales (*i.e.* spectral index $-2 \lesssim n \lesssim -1$), the distribution of $M \sim 10^8\text{--}10^9 M_\odot$ halos is a steep function of mass ($d \ln N / d \ln M \approx -2$) and the bulk of the halos are expected to form at $z \gtrsim 3$. Under “ordinary” conditions, the gas in these halos would rapidly cool, collect in the cores and undergo star-formation. Studies of Ly α clouds, however, suggest that the universe at high redshifts is permeated by an intense metagalactic UV flux. This UV background will photoionise the gas and hence prevent it from cooling and collecting in the cores of low mass halos until $z \lesssim 2$ when the photoionising background begins to decline rapidly (Babul & Rees 1992; Quinn, Katz, & Efstathiou 1996). In our model, the power spectrum of density fluctuations that grow into halos of circular velocity less than 35 km s^{-1} is described by the standard cold dark matter (SCDM) power spectrum normalized such that the rms density fluctuations on the scale of $8h^{-1}\text{Mpc}$ are $\sigma_8 = 0.67$. The comoving number density of minihalos existing at $z \approx 1$, estimated using the analytic Press-Schechter (1974) formalism, is

$$\frac{dN}{d \ln(M)} \approx 2.3 \left(\frac{M}{10^9 M_\odot} \right)^{-0.9} \text{ Mpc}^{-3}. \quad (1)$$

The mass function of dwarf galaxies is thus fixed with no free parameters. Once the gas in dwarf galaxy halo can recombine and cool, star-formation occurs rapidly, ceasing at 10^7 years (the typical lifetime of massive stars) when supernova explosions heat and expel the gas. The probability of such a burst occurring in a dwarf galaxy is assumed to decline exponentially with redshift from $z = 1$, with the timescale ($t^* = 2 \times 10^9 \text{ yr}$) fixed by the requirement that the model must match the observed B-band redshift distribution of Glazebrook et al. (1995).

Apart from the dwarf-galaxy mass function, which is fixed, the three most important parameters of the model are (1) star-formation efficiency ¹, assumed to be 10%, (2) t^* , the burst probability timescale, and (3) the redshift, z_f , at which the dwarfs start to form stars — which could plausibly be as high as $z = 1.5$ and as low as $z = 0$ and could vary as a function of mass. The choice of these parameters is discussed by Babul & Ferguson (1996); they have not been adjusted to fit the HDF data.

¹Babul & Ferguson (1996) incorrectly computed the total stellar mass for their dwarf galaxies; their assumed star-formation efficiency of 30% resulted in luminosities a factor of 2.8 too high, for the adopted IMF. To make the results directly comparable, we have kept the same total luminosities for the dwarf galaxies, but lowered the corresponding star-formation efficiency to 10% (for a Salpeter IMF from 0.1 to $100 M_\odot$). Nevertheless, as most of the light is produced by massive stars and most of the stellar mass is in low-mass stars, the conversion from dwarf-galaxy mass to dwarf-galaxy luminosity carries with it large uncertainties.

The parameters for the giant galaxies in the model are similar to those used in pure luminosity evolution (PLE) studies (Yoshii & Takahara 1988; Rocca-Volmerange & Guiderdoni 1988; Pozzetti, Bruzual, & Zamorani 1996). The luminosity functions for the giants (E through Sdm) are Gaussian, tuned to approximate the type-dependent luminosity functions given by Binggeli, Sandage, & Tammann (1988). The bulge/disk total mass ratios and scatter are tuned for each type to match the observations of Simien & de Vaucouleurs (1986) for local galaxies. This combination of parameters has been shown (Babul & Ferguson 1996) to provide a good fit to the overall luminosity function from the APM survey (Loveday et al. 1992).

The parameters of the different distribution functions are summarised in Table 1, and described in more detail in Babul & Ferguson (1996). Table 1 lists, for each galaxy type: N_0 , the co-moving space-density integrated over the entire luminosity function; the characteristic absolute magnitude (M_{BJ} for the Gaussian luminosity functions, M_{BJ}^* for the Schechter function, and M_0 for the power-law mass function used for the dwarfs); the width of the Gaussian luminosity function σ or the power-law exponent α of the faint-end of the luminosity function; the mean bulge/total luminosity ratio in the B_J band and the Gaussian scatter σ about that mean; the redshift of formation z_f , or maximum redshift of formation z_{max} ; and the e -folding timescales of star-formation of bulge and disk.

Upon formation, all galaxies (giants and dwarfs) evolve only in their stellar populations. That is, there is no merging and there are no subsequent bursts of star formation. The different colours of present-day giant galaxies are reproduced by adjusting the star-formation timescale (e -folding time) of the model. Galaxy disks form stars at roughly constant rate from $z = 5$ to $z = 0$. Bulges form stars in a burst of duration 2×10^8 years.² Spectral evolution is computed using the Padova isochrones (Bertelli et al. 1994) and stellar atmosphere models. The intrinsic spectra of the galaxies are attenuated by the mean expected intergalactic HI absorption using the models of Madau (1995). This attenuation has a significant effect on the predicted numbers and colours of galaxies with $z > 2.5$ (Madau et al. 1996).

²The e -folding time of the initial star-formation episode adopted in this paper is revised from that adopted by Babul & Ferguson (1996), and is the average of the timescales for the onset of galactic winds from the various models reviewed by Gibson (1996).

2.2. The $q_0 = 0.01$, Pure Luminosity Evolution

The $q_0 = 0.01$ model is identical to the above model with two exceptions. First, there is much more volume at high redshift in the low q_0 model, and hence more high-redshift galaxies are predicted per unit area on the sky. Second, the model does not include the large population of boojums turning on at $z \approx 1$. Instead the faint end of the luminosity function is populated by galaxies with a star-formation timescale of 3×10^{10} yr and a Schechter (1976) luminosity function with parameters $\alpha = -1.3$ and $M_B^* = -16$, and an integrated co-moving density $n_0 = 0.2 \text{ Mpc}^{-3}$ from 3.5×10^{-3} to $10L^*$. In other words, the faint-end of the luminosity function is modeled as a population of dwarf irregular galaxies with a luminosity function slope intermediate to the flat value measured by Loveday et al. (1992) and Lin et al. (1996) and the steeper values measured in the CfA redshift survey (Marzke, Huchra, & Geller 1994) and in nearby clusters (De Propis et al. 1995). It should be noted that similar models PLE (Pozzetti et al. 1996; Yoshii & Peterson 1994), have been shown to provide a reasonable fit to the ground-based counts and redshift distributions, provided q_0 is low. However, this may have been to a certain extent fortuitous, as none of the previous models included intergalactic absorption, which could in principle have a significant effect on the counts and colours of faint galaxies (Madau 1995).

2.3. Simulations and Galaxy Photometry

Having set all the distribution functions and evolutionary parameters, a Monte-Carlo procedure is used to produce a list of galaxy redshifts, masses, ages, bulge r_e and disk α (in kpc and arcsec), and magnitudes in various bands (for bulge and disk components, as well as the total) for each of the galaxies. Magnitudes are computed by integrating the properly redshifted and k -broadened spectra for the bulge and disk components through the filter bandpasses given in the HST WFPC-2 handbook (Biretta 1995) as implemented in the IRAF synphot task.

These catalogs of simulated galaxies are used as input to the IRAF ardata task to construct simulated images of the HDF. A noiseless image of the model galaxies in each band is constructed and convolved with the HST point-spread function (measured from the unsaturated blue star near the center of chip 4 in the real observations). We have simulated only the wide field (WF) chips for the comparisons, adopting the plate scale (0.04 arcsec/pixel) of the HDF “drizzled” images (Williams et al. 1996). A separate noise image is constructed from a model that includes Poisson errors on the sky background and readout noise for each of the exposures. This noise image is convolved with the drizzled noise kernel given in Williams et al. (1996), scaled to the pixel size in the final drizzled image (by

multiplying by 0.4), and multiplied by a factor of 1.1 to account for the stochastic loss of exposure time in each pixel due to cosmic-ray rejection. The contribution from Poisson errors on counts from the objects is not included, but is negligible for objects near the sky level. The scaled noise image is then added to the noiseless object image to produce the final simulated image. This prescription reproduces the noise properties of the real HDF images remarkably well, as can be seen by examination of the simulated images in Figures 1-3, and by detailed comparison of image statistics on different scales.

For quantitative comparisons, analysis of the images is carried out using the FOCAS galaxy detection and photometry software (Jarvis & Tyson 1981; Valdes 1982; revised by Adelberger & Steidel 1996). The detection algorithm, as applied to the HDF images, is discussed by Williams et al. (1996). Briefly, objects with S/N greater than 4σ within a contiguous area of 25 pixels (each 0.04 square arcseconds in area) are considered detections. Isophotal magnitudes are estimated by summing the sky-subtracted counts within the detection isophote. For a point source on the WF, this minimum area encompasses roughly 60% of the total object flux. FOCAS total magnitudes are computed from the total counts within an area that is a factor of two larger. The photometry of the simulated images and the HDF images is identical, except for one minor difference. For the HDF images, the individual pixels are weighted by the inverse variance, to account for the small differences in exposure time between adjacent pixels in the sub-sampled image. For the simulations, the exposure time is assumed to be constant for all pixels. This difference is likely to be unimportant, as the variations in exposure time between pixels in the real HDF images are typically less than 20%.

In the case where there are multiple peaks within the initial detection isophote, FOCAS computes photometric parameters for both the “parent” and “daughter” objects. Because we only want to count objects once, we have to decide, for each object, whether to keep the parent or the daughters. For both the true HDF images and the simulations, we have adopted the separation and colour criteria of Williams et al. (1996), keeping the parent if the daughters have $\Delta(V_{606} - I_{814}) < C$, and separation $S_{ij} < F \times (r_i + r_j)$, with $C = 0.3$ mag and $F = 5$, and r_i and r_j are galaxy radii determined from the FOCAS isophotal areas as $r_i = \sqrt{A/\pi}$. In the real HDF images, galaxy counts are only mildly affected by the choice of whether to count parents or daughters, growing by 20% if all the subcomponents (daughters) rather than the parents are counted as individual objects (Williams et al. 1996). The two main issues that may affect the comparison of our models to the real images are (1) clustering on small scales, and (2) substructure within galaxies. Galaxy positions in our simulations are stastically independent. Intrinsic clustering in the real universe is likely to lead to a reduction in counts, as overlapping objects will in some cases be counted as one object. The Villumsen, Freudling, & da Costa (1997) analysis of the angular correlation

function in the HDF suggests that clustering will lead to an excess probability of about 10% for galaxies to have a separation of 1 arcsec. Hence, we expect that clustering will lead to only a very slight undercounting of galaxies. (Note that the higher probability found by Colley et al. (1997) applies only to galaxies with photometric redshifts $z > 2.4$, and their analysis used a different algorithm for counting galaxies and merging subcomponents.)

Substructure within galaxies will work in the opposite direction. Galaxies in our models have smooth profiles, while real galaxies, especially those being observed at rest-frame UV wavelengths, tend to have substructures. Even with the merging algorithm described above, it is likely that some individual galaxies in the real HDF have been counted as multiple objects.

These effects, while ultimately of great interest, have only a mild effect on the counts. The change in luminosities of the individual components compensates for the change in the number of components. Thus both the slope and normalization of the faint counts stays approximately the same. The effect on galaxy colors and size distributions is likely to be larger, but we have not attempted to model it in this paper. The gross differences between the models and the data, described below, are likely to be relatively insensitive to the details of the merging and splitting algorithms, although further investigation is certainly warranted.

3. Redshift Distributions

The $q_0 = 0.01$ model and the dwarf-dominated $q_0 = 0.5$ model, while rather similar in their predicted redshift distributions to ground based limits, differ dramatically in their predicted redshift distributions at the depths probed by the HDF images. Figures 4 and 5 show the model redshift distributions compared to the Canada-France redshift survey (CFRS; Lilly et al. 1995), and the predicted redshift distributions in two fainter magnitude slices. In the CFRS magnitude range ($17.5 < I_{AB} < 22.5$), the predicted distribution for both models provide a reasonable match to the data for $z < 2$ *given the incompleteness of the sample*. In the $q_0 = 0.5$ model, 25% of the galaxies (most right near the CFRS magnitude limit) have $z > 2$, which is just compatible with the 81% completeness of the sample. The high-redshift tail in this magnitude range is much less pronounced for the low q_0 model because the luminosity-distance is larger at high redshift.

At fainter magnitudes, the dwarfs in the $q_0 = 0.5$ model dominate the counts and the redshift distributions. While the vast majority of the dwarfs form their stars at redshifts $0.5 < z < 1$ in the model, the counts and redshifts are dominated by faded dwarf galaxies

at lower redshifts. This is root of the problems with matching the distributions of colour and radius described in the next section. In the low q_0 model, the redshift distribution at HDF magnitudes $24 < I_{814} < 27$ is dominated by high-redshift bulges and ellipticals. The redshift distribution is much more uniform at fainter magnitudes $27 < I_{814} < 29$. The peak is missing at high redshift because most of the ellipticals and bulges are brighter than $I_{814} = 26$ during the epoch of rapid star formation. The ellipticals and bulges that appear in the faint magnitude cut come from the faint tail of the adopted Gaussian luminosity function. For redshifts $z < 2$, faint sample is dominated by late-type low-luminosity galaxies, which in this model are forming stars at roughly constant rates.

4. Comparisons to HDF Observations

In Figures 2 and 3, we show simulated F814W HDF images for the dwarf-dominated model and the low q_0 model, respectively. In Figure 1, we show the HDF image. A visual comparison of the images reveals that the image for the dwarf-dominated model appears to have more galaxies than in the HDF image, this impression being primarily due to the large number of extended, low surface brightness galaxies near the detection limit that are not present in the HDF image. The bulk of the galaxies in the HDF image are more point-like. In contrast, the faintest galaxies in the image for the low q_0 model are similar in size to those in the HDF image. However, the simulated image does not appear to have as many galaxies.

The model counts are compared to the observations in figures 6 and 7, where we show, for the model, the underlying counts based on true total magnitudes (dashed line), and the measured counts based on FOCAS isophotal magnitudes (solid line) and “total” magnitudes. Note the rather striking differences between the underlying counts and the FOCAS measured counts for both models. These differences justify our suspicion that selection and photometry biases are important at faint magnitudes, and must be included for a fair assessment of the predictions for *any* galaxy-evolution model.

The $q_0 = 0.5$ dwarf-dominated model clearly overpredicts the counts at HDF magnitudes, even when selection biases are taken into account (Fig 6). The excess is the most striking in the I_{814} band, although it appears at faint magnitudes in all bands. The excess is largely due to fading dwarf galaxies, rather than dwarf galaxies at the peak of their starformation activity. The model predictions for the $q_0 = 0.01$ model are a better match, being largely successful in the I_{814} band, while underpredicting the counts at relatively bright B_{450} magnitudes. This latter discrepancy is related to the large surface-density of high-redshift galaxies predicted by the model, and shows up as well in the colour

distributions discussed below. Note that this discrepancy would not have been seen in earlier PLE models, which did not include the attenuation of the intergalactic medium (Yoshii & Takahara 1988; Gronwall & Koo 1995; Pozzetti et al. 1996).

The distribution of radii are compared in Figure 8. The radii plotted are first-moment radii measured by FOCAS within the detection isophotes.³

The observed distribution peaks at 0.2 arcsec in the magnitude range $24 < V_{606} < 27$, and at about 0.15 arcsec in the range $27 < V_{606} < 29$. These distributions of radii are almost perfectly matched by both models at the brighter magnitudes, and by the low q_0 model in the fainter magnitude bin. However, in spite of being dwarf-dominated, the $q_0 = 0.5$ model predicts galaxies that are systematically *larger* than observed at the faintest magnitudes.

Figure 9 compares the $B_{450} - I_{814}$ colours for the models and data. While the peaks in the model colour distributions roughly agree with the observations, neither model provides a very good match to the overall distributions. The $q_0 = 0.5$ model has a blue peak in the brighter magnitude bin that is not observed, while it predicts a red tail similar to that seen in the real HDF images. At fainter magnitudes ($27 < I_{814} < 29$) there is no blue peak, and hence the model predicts a narrower distribution than observed. The $q_0 = 0.01$ model does not have enough blue galaxies at the brighter magnitudes, and greatly overpredicts the number of very red galaxies ($B_{450} - I_{814} > 2$). At fainter magnitudes the distribution is a better match, but there is still an excess of very red galaxies relative to the observations.

The differences reflect both the different redshift distributions of the models, and the different proportions of galaxies undergoing star-formation at moderate redshifts. During the starburst phase, the dwarfs in the $q_0 = 0.5$ model show up as nearly flat spectrum objects, giving rise to the blue peak in the magnitude range $24 < I_{814} < 27$. There are few galaxies in the HDF with colours this blue. At fainter magnitudes, the colour distribution is dominated by faded, lower-redshift remnants of the starburst epoch. The blue tail is missing because there are no dwarf galaxies in the model with star-formation rates less than $1.8 M_{\odot}$ per year. This is due the cutoff of the dwarf-galaxy mass function at 15 kms^{-1} . Lower mass potentials are not deep enough to retain 10^4 K gas during the formation epoch. While the lower mass cutoff has a physical justification, the adopted star-formation efficiency of 10%, and star-formation timescale of 10^7 years are not highly constrained. Thus it is

³ The FOCAS first-moment radius is defined as

$$r_1 = \sum rI(x, y) / \sum I(x, y), \quad (2)$$

where $I(x, y)$ is the intensity in each pixel within the detection isophote.

may be possible to achieve a better match to the colour distribution without revising the fundamental assumption that dwarf galaxies are dominating the counts.

For the low q_0 model, the most serious discrepancy is the prediction that there should be a large population of very red galaxies, primarily in the brighter magnitude bin, but extending also to the faintest magnitudes seen in the HDF. This red tail is due to bulges and ellipticals forming stars at $z > 3.5$. It is an extremely robust prediction of the models that such galaxies should have red $B_{450} - I_{814}$ colours, since the colours are determined largely by the intrinsic Lyman limits in galaxies, and by absorption due to intervening Lyman α clouds (Madau 1995). In the bright magnitude bin, the low q_0 model, even ignoring the very red tail, is skewed to the red of the observed distribution. It is apparently underabundant in star-forming galaxies at moderate redshifts. At fainter magnitudes, the colour distribution is a more reasonable match to the observations, with a higher proportion of blue objects. This is in part explained by the virtual disappearance of passively evolving ellipticals from the sample at moderate redshifts, because the observations have gone beyond the peak of the assumed Gaussian luminosity functions. The counts are thus dominated by star-forming galaxies.

Figure 10, reproduced from Madau et al. (1996), shows colour-colour diagrams for galaxies on the three WF chips in the HDF. The dashed lines show regions designed to select galaxies in the redshift range $2.3 < z < 3.5$ (in the $U_{300} - B_{450}$ vs. $B_{450} - I_{814}$ plane shown in Fig. 10a) and $3.5 < z < 4.5$ (in the $B_{450} - V_{606}$ vs. $V_{606} - I_{814}$ plane in Fig. 10b). Galaxies within these regions are very likely to be star-forming (relatively blue) galaxies at high redshifts that have “dropped out” of the bluer band due to Lyman limit and intergalactic Ly α absorption. The number of dropouts seen and predicted by the models are listed in Table 2. It is interesting and important to note that this prediction is *extremely sensitive* to biases in the selection and photometry of galaxies within FOCAS. Because the counts of high-redshift galaxies in both models are steep at faint magnitudes, the ~ 0.5 mag difference between FOCAS isophotal magnitudes and the model galaxy total magnitudes can introduce large differences in the predicted number of dropout galaxies. These differences are largely taken into account by using FOCAS on the simulated images, but our conclusions below must certainly be tempered by the lack of knowledge of the true surface-brightness profiles of high-redshift galaxies.

The predictions of the dwarf-dominated $q_0 = 0.5$ model are shown in Fig. 11. The model underpredicts the number of U-band dropouts and overpredicts the number of B-band dropouts. The discrepancy is significantly worse for the low q_0 model (Fig. 12), which greatly underpredicts the number of U dropouts, and greatly overpredicts the number of B dropouts. Furthermore, for both models, B dropouts are seen at magnitudes

considerably brighter than those observed.

The differences between the two models can be understood as follows. The volume at high redshifts is considerably higher in the low q_0 model, leading to a higher surface density of objects projected on the sky. Thus, for the same local density and redshift of formation, a low q_0 model predicts more sources near $z = 5$ than a $q_0 = 0.5$ model. However, there is also more time between redshifts of 3 and 5 in the low q_0 model (1.6 Gyr) than in the $q_0 = 0.5$ model (0.7 Gyr). Therefore galaxies that form at $z = 5$ have more time to fade in the open model, and, if the star-formation timescale is sufficiently short, can fade and redden sufficiently that they do not meet the U-dropout selection criteria. The specific predictions are very sensitive to the assumed redshift of formation and duration of the star-forming epoch, points to which we will return in the next section.

There are significant discrepancies between the models and the observations in other parts of these diagrams as well. In particular, during the burst phase, the dwarfs in the $q_0 = 0.5$ model populate a region slightly blueward of flat spectrum (in the lower left corner of Fig. 11a). There are virtually no galaxies in this region in the HDF data.

The heavy concentration of galaxies at ($0 < U_{300} - B_{450} < 0.5$; $B_{450} - I_{814} \approx 0.5$) is not present in either model. Galaxies in this portion of the diagram are likely to lie in the redshift range $1 < z < 2$.

5. Discussion

As outlined in the introduction, our purpose in this paper is to examine the constraints imposed on the bursting-dwarf model by the Hubble Deep Field observations. By way of comparison, we perform the same analysis on a standard low q_0 PLE model, to highlight the differences between the predictions of the models, and the discriminatory power of these deep images. Both types of models have been shown previously to provide a reasonable fit to ground-based counts and redshift distributions. The preceding sections have presented a detailed comparison of these models to the HDF data. The comparisons have highlighted (a) the importance of including selection biases into the comparisons of models to the HDF data, (b) the large differences in the predicted counts and colour distributions for these two rather different models, and (c) the failure of either model to reproduce the observations.

The most important discrepancy for the low q_0 PLE model is the prediction of a substantial number of $z > 3.5$ galaxies at relatively bright magnitudes. Previous PLE models (Gronwall & Koo 1995; Pozzetti, Bruzual, & Zamorani 1996) have shown reasonable agreement with ground-based data in the magnitude range $24 < B < 26$, where we see the

discrepancy, but this may have been fortuitous, as these models did not include the effects of intergalactic absorption, which is clearly important at faint magnitudes in the U and B bands. The number and brightness distribution of high-redshift galaxies is sensitive to the redshift of formation z_f , the star-formation timescale, the stellar initial mass function, and the amount and distribution of dust in young galaxies. Thus it is not possible to rule out PLE models simply on the basis of the overprediction of $z > 3.5$ galaxies. However, simply hiding these galaxies is not sufficient to reconcile the model to the observations because then the PLE model will substantially underpredict the counts. The most straightforward solution, of course, is to posit different redshifts of formation for different types of galaxies, or to incorporate merging into the model. Such possibilities are certainly viable, but are no longer in the spirit of PLE models.

The disagreement between the $q_0 = 0.5$ dwarf-dominated model and the HDF observations can be largely attributed to the overproduction of faded remnants. The model counts near the HDF limits are dominated by low-redshift non-starforming dwarfs. These remnants are both redder and larger than the typical galaxies seen in the HDF. There are two plausible modifications to the model which might reconcile it to the observations without contradicting the underlying assumptions of $q_0 = 0.5$, a CDM mass-spectrum for the dwarfs, and a redshift of formation governed by the ionisation history of the universe. The first is that the formation epoch of the dwarfs could extend to higher redshifts than we have assumed (possibly up to $z = 1.5$), and could depend on galaxy mass. This would allow the boojums to be brighter and leave them more time to fade. The second is that the initial mass function in the boojums could be skewed toward high mass stars, or truncated at some fairly high lower mass limit. The skewed IMF would cause the dwarfs to fade faster, possibly curing the problem of remnants at low redshifts.

In a broader sense, the HDF observations clearly provide new and important constraints on galaxy-evolution models. At the faint magnitudes probed by these observations, the problems with the simple models discussed in this paper are particularly acute. It is difficult to tell at present whether the problems lie in the details (e.g. the IMF, dust content, metallicity distributions) or in the fundamental assumptions (e.g. that merging is unimportant, or that giant galaxies all began forming at roughly the same time, with different star-forming rates). It is clear that further modeling of the growing database of galaxy properties in this small patch of sky, with careful attention to selection effects, has the potential to discriminate between widely different world models that heretofore seemed equally plausible.

This paper is based on observations made with the Hubble Space Telescope; support for this work was provided in part by NASA through Hubble Archival Research grant

#AR-06337.20-94A awarded by Space Telescope Science Institute, which is operated by the Association of Universities for Research in Astronomy, Inc., under NASA contract NAS5-26555. A.B. is grateful for support through the Bergen Career Award from the Dudley Observatory. We would like to acknowledge Bob Williams and the STScI HDF team for their efforts in planning and carrying out the HDF observations. We acknowledge in particular Mark Dickinson, Andy Fruchter, Mauro Giavalisco, and Piero Madau for many fruitful discussions and collaborations on the HDF and galaxy evolution.

Table 1: Giant Galaxy Parameters

Type	Luminosity Function			Bulge/Total Ratio			z_f	τ_{Bulge}	τ_{Disk}
	$N_0(\times 10^{-3}\text{Mpc}^{-3})$	$\langle M_{\text{BJ}} \rangle$	σ	mean	σ				
E	0.37	-18.70	1.7	1.0	0.0	5	0.2	—	
S0	1.15	-18.70	1.7	0.4	0.25	5	0.2	1	
Sab	2.00	-19.96	1.1	0.3	0.27	5	0.2	30	
Sbc	4.00	-18.48	1.3	0.15	0.27	5	0.2	30	
Sdm	8.00	-16.00	1.3	0.0	0.0	5	—	30	

Additional late-type dwarfs for low q_0 model								
Type	$N_0(\times 10^{-3}\text{Mpc}^{-3})$	M_{BJ}^*	α	mean	σ	z_f	τ_{Bulge}	τ_{Disk}
Irregular	200	-16.00	-1.3	0.0	0.0	5	—	30

Bursting dwarfs for $q_0 = 0.5$ model								
Type	$N_0(\times 10^{-3}\text{Mpc}^{-3})$	M_0	α	mean	σ	z_{max}	τ_{Bulge}	SF duration
Boojum	4000	$10^9 M_{\odot}$	-2	0.0	0.0	1	—	0.01

Table 2: Numbers of U_{300} and B_{450} band Dropouts

Data set	U dropouts	B dropouts
HDF	58	14
$q_0 = 0.5$	30	41
$q_0 = 0.01$	2	172

References

- Adelberger K., Steidel C. C., 1996, private communication
- Babul A., Ferguson H. C., 1996, *ApJ*, 458, 100
- Babul A., Rees M., 1992, *MNRAS*, 255, 346
- Bertelli G., Bressan A., Chiosi C., Fagotto F., Nasi E., 1994, *A&AS*, 106, 275
- Binggeli B., Sandage A., Tammann G. A., 1988, *ARA&A*, 26, 509
- Biretta J., 1995, *WFPC-2 Instrument Handbook*. STScI, Baltimore
- Cole S., Aragon-Salamanca A., Frenk C. S., Navarro J. F., Zepf S. E., 1994, *MNRAS*, 271, 781
- Colley W., Gnedin O., Ostriker J. P., Rhoads J. E., 1997, *ApJ*, 488, 579
- Cowie L. L., Songaila A., Hu E. M., Cohen J. G., 1996, *AJ*, 112, 839
- De Propis R., Pritchett C. J., Harris W. E., McClure R. D., 1995, *ApJ*, 450, 534
- Ellis R. S., Colless M., Broadhurst T., Heyl J., Glazebrook K., 1996, *MNRAS*, 280, 235
- Gibson B., 1996, *ApJ*, 468, 167
- Glazebrook K., Ellis R., Colless M., Broadhurst T., Allington-Smith J., Tanvir N., 1995, *MNRAS*, 273, 157
- Gronwall C., Koo D. C., 1995, *ApJ*, 440, L1
- Jarvis J. F., Tyson J. A., 1981, *AJ*, 86, 476
- Kauffmann G., Guiderdoni B., White S. D. M., 1994, *MNRAS*, 267, 981
- Lilly S. J., Le Fevre O., Crampton D., Hammer F., Tresse L., 1995, *ApJ*, 455, 50
- Lin H., Kirshner R. P., Schectman S. A., Landy S. D., Oemler A., Tucker D. L., Schechter P. L., 1996, *ApJ*, 464, 60
- Loveday J., Peterson B. A., Efstathiou G., Maddox S., 1992, *ApJ*, 390, 338
- Madau P., 1995, *ApJ*, 441, 18
- Madau P., Ferguson H. C., Dickinson M., Giavalisco M., Steidel C. C., Fruchter A. S., 1996, *MNRAS*, 283, 1388
- Marzke R. O., Huchra J. P., Geller M. J., 1994, *ApJ*, 428, 43
- Phillipps S., Driver S., 1995, *MNRAS*, 274, 832
- Pozzetti L., Bruzual G., Zamorani G., 1996, *MNRAS*, 281, 953
- Press W. H., Schechter P. L., 1974, *ApJ*, 187, 425

- Quinn T., Katz N., Efstathiou G., 1996, MNRAS, 278, L41
- Rocca-Volmerange B., Guiderdoni B., 1988, A&AS, 75, 93
- Schechter P., 1976, ApJ, 203, 297
- Simien F., de Vaucouleurs G., 1986, ApJ, 302, 564
- Valdes F., 1982, Faint Object Classification and Analysis System. KPNO Internal Publication
- Villumsen J., Freudling W., da Costa L. N., 1997, ApJ, 481, 578
- Williams R. E. et al., 1996, AJ, 112, 1335
- Yoshii Y., Peterson B., 1994, ApJ, 436, 551
- Yoshii Y., Takahara F., 1988, ApJ, 326, 1

Fig. 1.— Hubble Deep Field. The image shows an $80'' \times 80''$ portion of the field, in the F814W band, from the version 2 drizzled data (Williams et al. 1996).

Fig. 2.— Simulated Hubble Deep Field for the $q_0 = 0.5$ dwarf-dominated model. The image shows an $80'' \times 80''$ portion of the field in the F814W band.

Fig. 3.— Simulated Hubble Deep Field in the low- q_0 model. The image shows an $80'' \times 80''$ portion of the field in the F814W band.

Fig. 4.— Redshift distribution for the $q_0 = 0.5$ dwarf-dominated model. The top panel shows the measured redshift distribution from the CFRS survey (Lilly et al. 1995) as solid dots, the predicted distribution from the dwarf-dominated model as a histogram, and the prediction of a standard no-evolution model as a dotted curve. For the dwarf-dominated model the predicted distribution includes observational selection as described by Babul & Ferguson (1996). The model distributions are normalized to have the same total number of galaxies as the survey. The middle panel shows the predicted redshift distribution from the dwarf-dominated model in the magnitude range $24 < I_{814} < 27$. The bottom panel shows the same for $27 < I_{814} < 29$.

Fig. 5.— Same as Figure 4, for the low- q_0 PLE model.

Fig. 6.— Galaxy counts for the $q_0 = 0.5$ model as a function of AB magnitude in the F450W and F814W bands, together with a compilation of existing ground-based data. FOCAS isophotal and total magnitudes are shown as solid dots and X's, respectively. Model predictions based on total magnitudes (i.e. *without* accounting for observational selection or photometric biases) are shown as dashed lines. Model predictions from the FOCAS-generated catalogs of simulated galaxies are shown as solid lines. No colour corrections have been applied to the ground-based data. For the typical colours of galaxies in the HDF, the colour corrections are less than 0.1 mag.

Fig. 7.— Same as Fig. 6, for the low q_0 model.

Fig. 8.— Distribution of radii for both models, compared to the data. The radii for both the models and the data are the first-moment radii measured by FOCAS. The HDF measurements are shown as histograms with Poisson error bars. The model predictions are the light solid curves.

Fig. 9.— Distribution of $B_{450} - I_{814}$ colours for both models, compared to the data. The colours for both the models and the data are from FOCAS measurements of the images. The HDF measurements are shown as histograms with Poisson error bars. The model predictions are the light solid curves. For both the models and the data there are galaxies that are detected in the F814W image but not in the F450W image. For these galaxies, the colour is assigned from the 1σ lower limit to the B_{450} magnitude. The hashed regions indicate portion of the diagrams populated by these lower limits. Hashes slant in opposite directions for the models and the data.

Fig. 10.— (a) $U_{300} - B_{450}$ vs. $B_{450} - I_{814}$ colour-colour plot of galaxies in the HDF with $B_{450} < 26.8$. Objects undetected in F300W (with signal-to-noise < 1) are plotted as triangles at the 1σ lower limits to their $U_{300} - B_{450}$ colours. Symbol size scales with the I_{814} magnitude of each object. The dashed lines outline the selection region within which we identify candidate $2 < z < 3.5$ objects. Details of the selection criteria are given by Madau et al. (1996). (b) $B_{450} - V_{606}$ vs. $V_{606} - I_{814}$ colour-colour plot of galaxies in the HDF with $V_{606} < 28.0$. Meanings of the symbols are the same as in the previous plot. The dashed lines bound the region that isolates galaxies with $3.5 < z < 4.5$.

Fig. 11.— Same as Figure 10, for the $q_0 = 0.5$ dwarf-dominated model. Galaxy magnitudes are from FOCAS measurements, as for the data.

Fig. 12.— Same as Figure 11, for the $q_0 = 0.01$ PLE model. Galaxy magnitudes are from FOCAS measurements, as for the data.

Figs 1-3 are in separate files.

Figure 4.
Redshift distributions for $q_0 = 0.5$ dwarf-dominated model

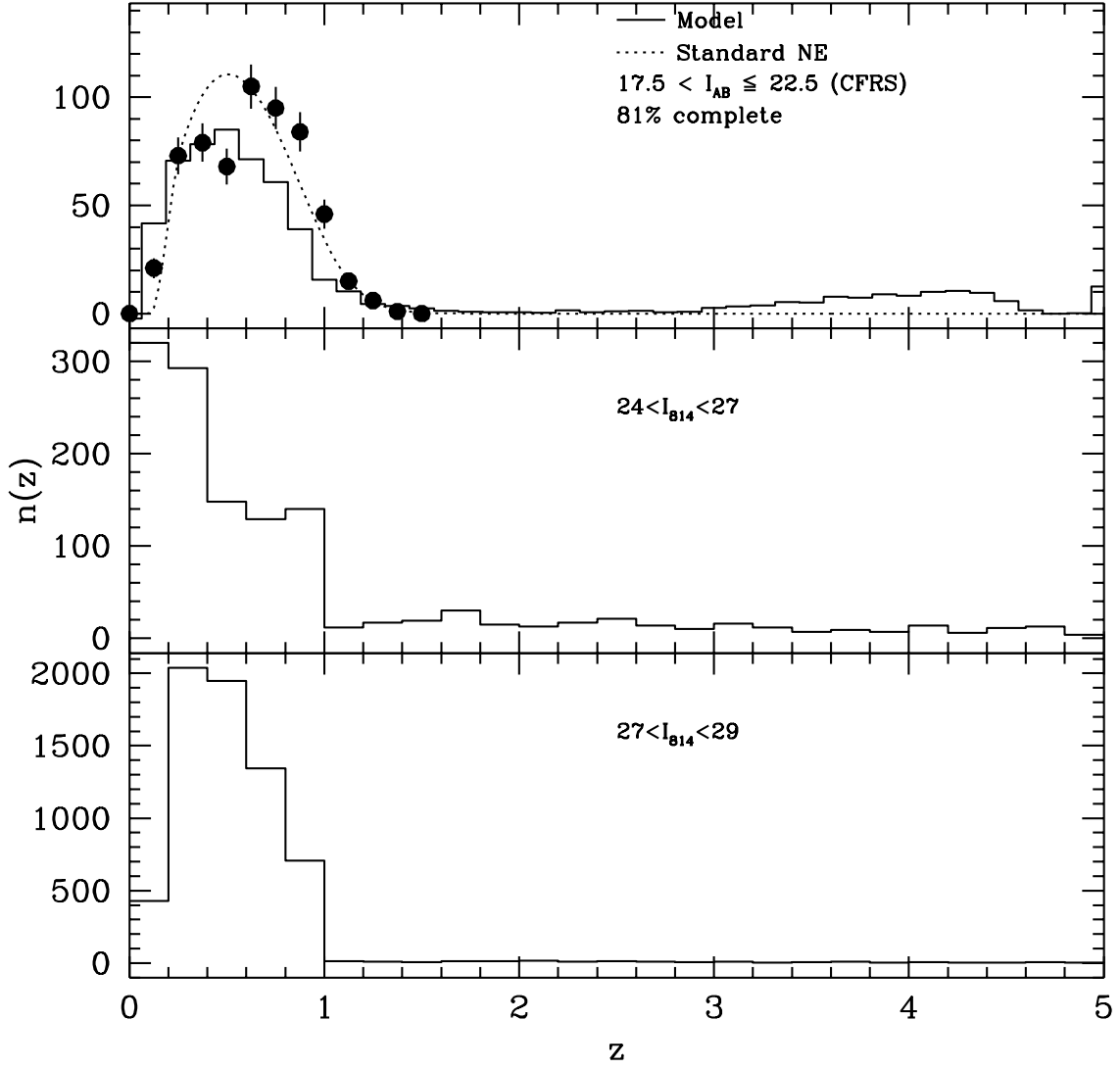


Figure 5.
Redshift distributions for $q_0 = 0.01$ model

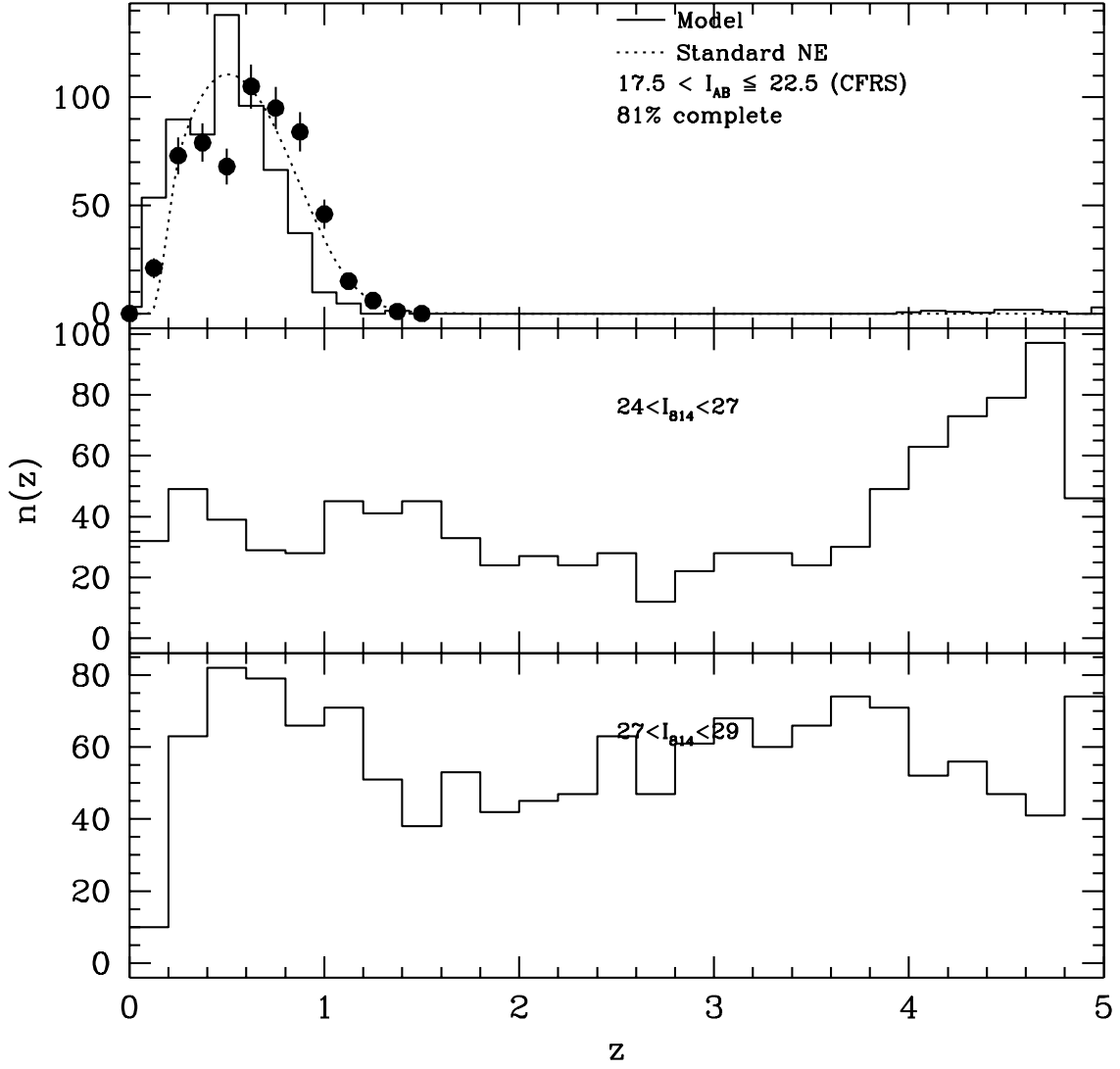


Figure 6.
 I_{814} AB Magnitude

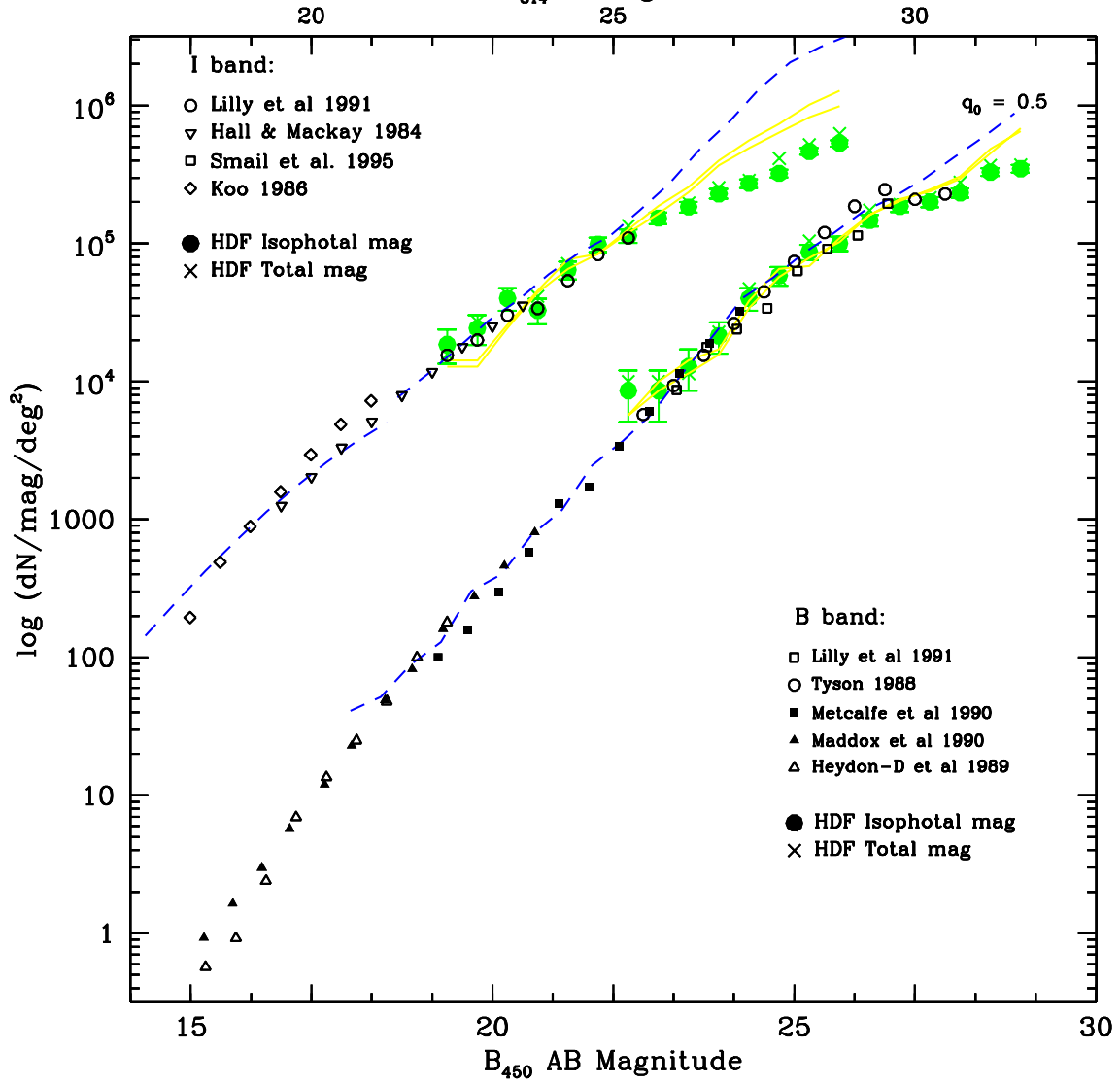


Figure 7.
 I_{814} AB Magnitude

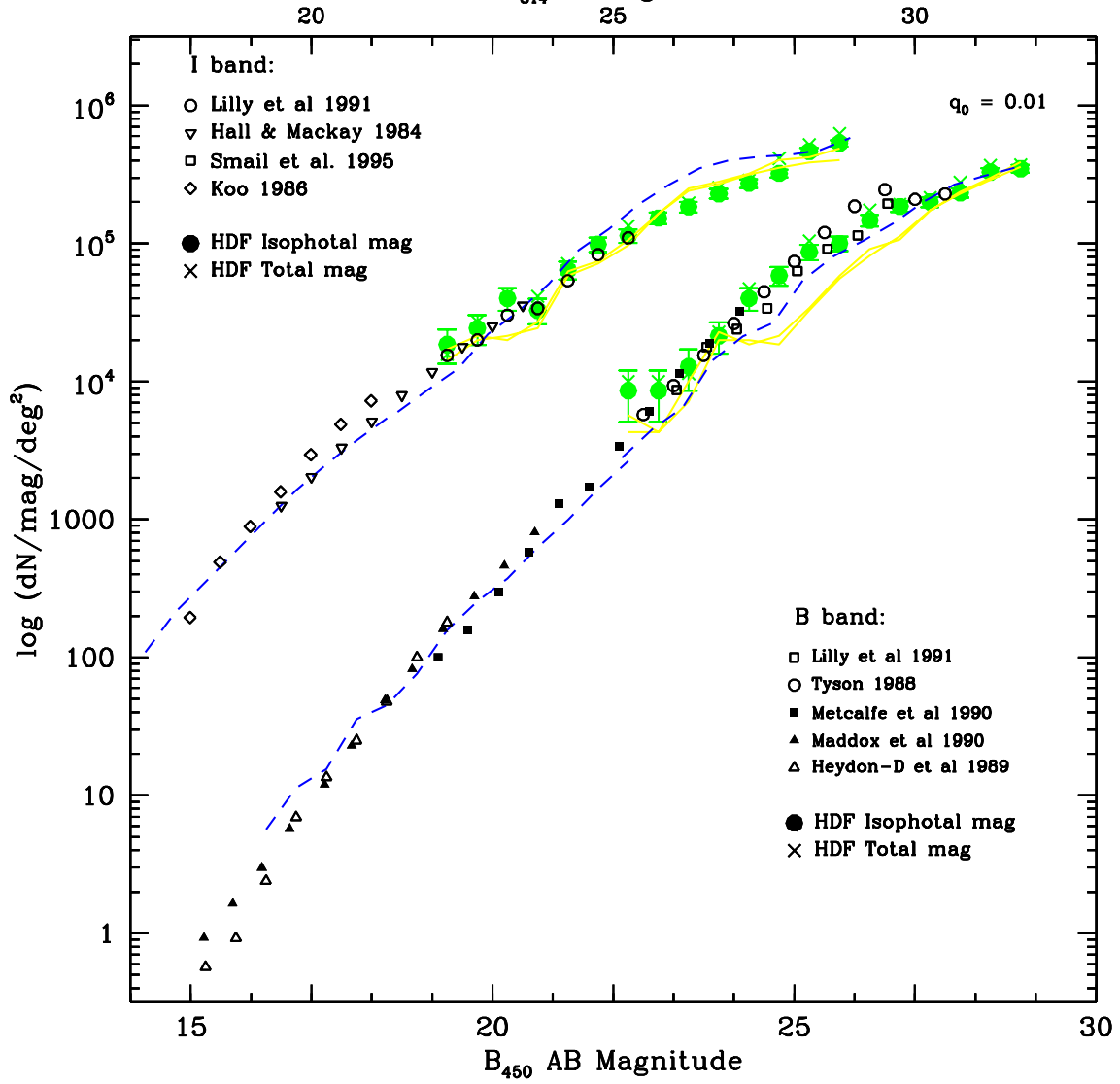


Figure 8.

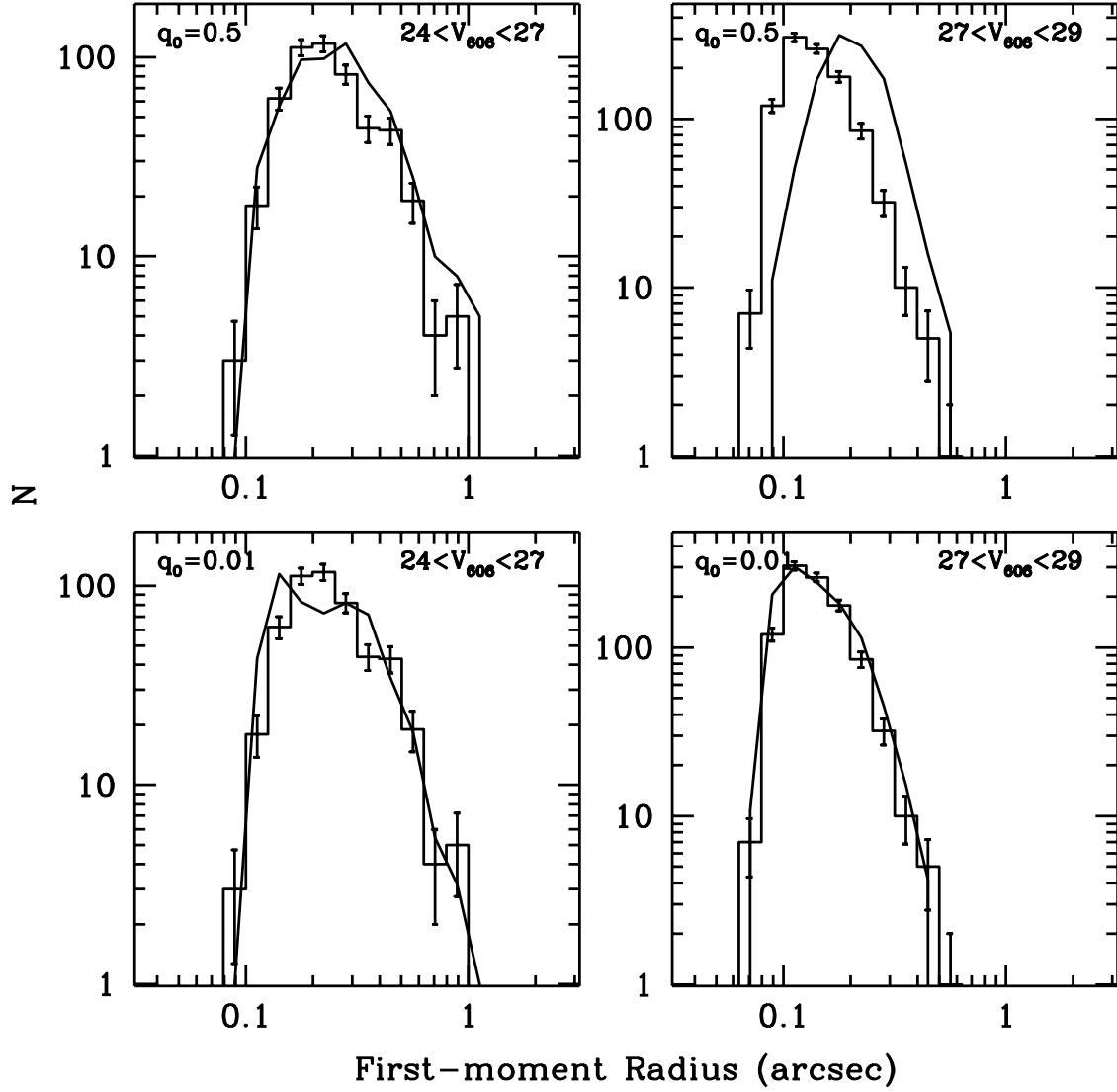


Figure 9.

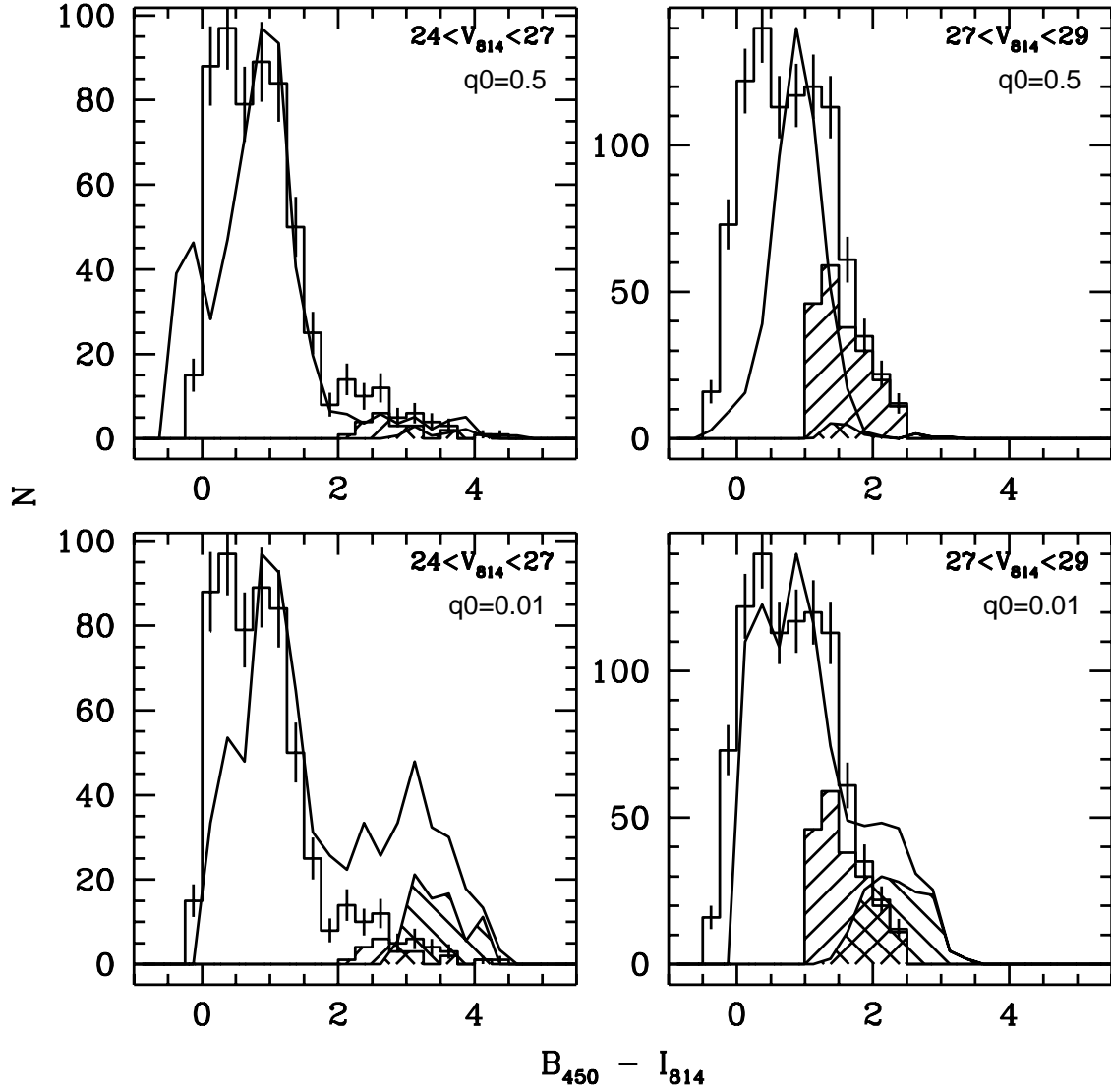


Figure 10a.
HDF WF1-3

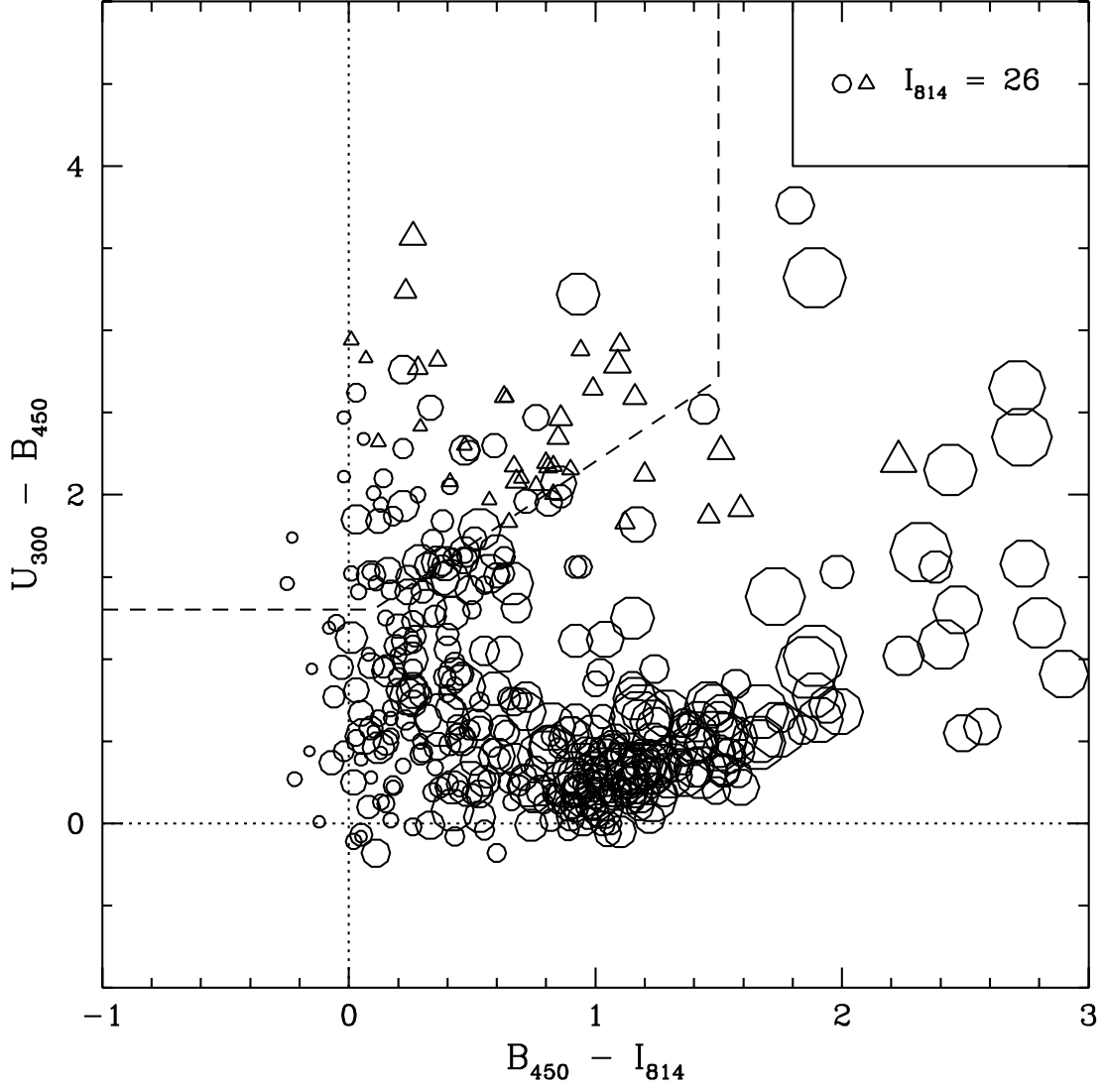


Figure 10b.
HDF WF1-3

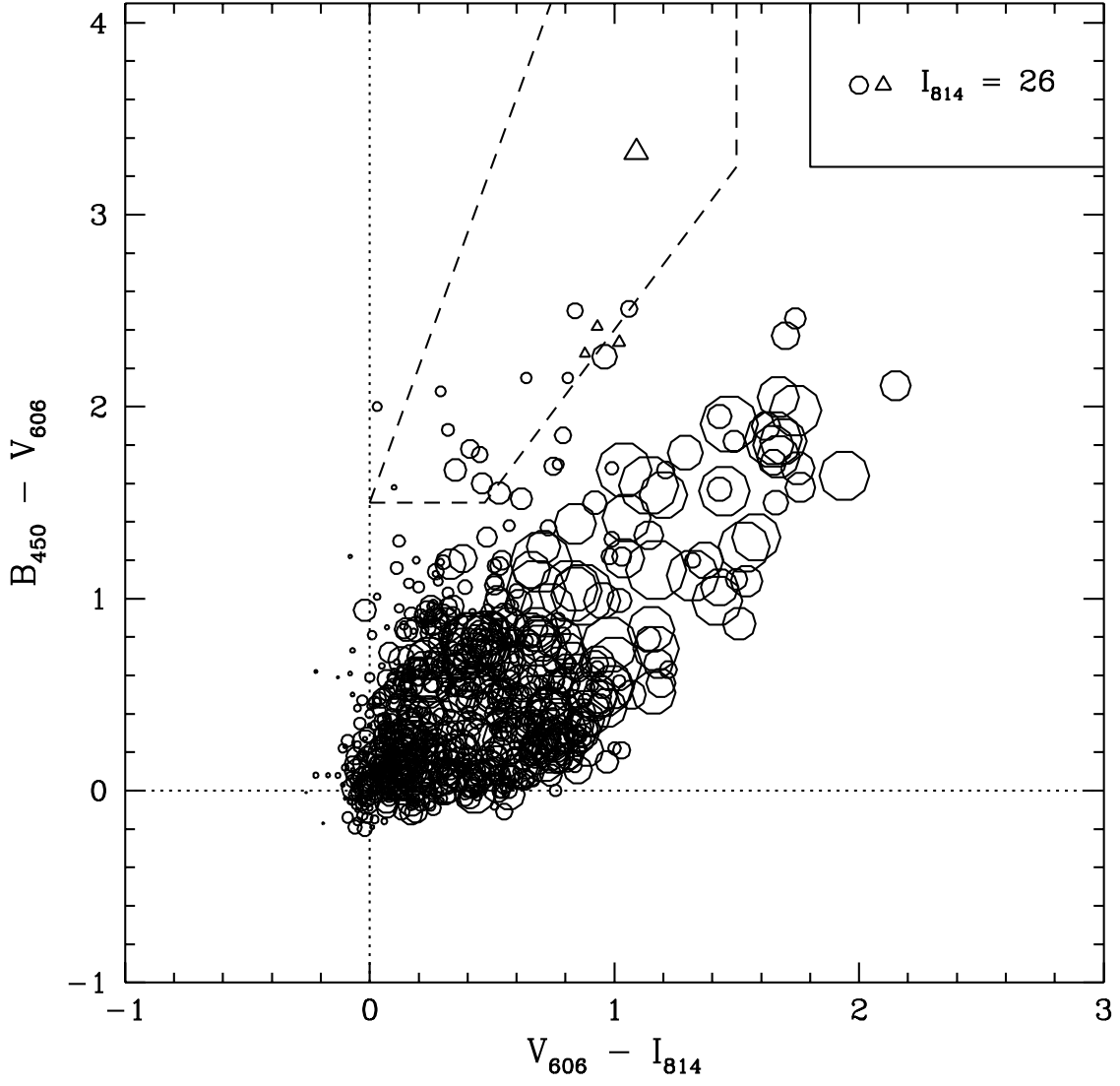


Figure 11a.
 $q_0=0.5$ dwarf-dominated

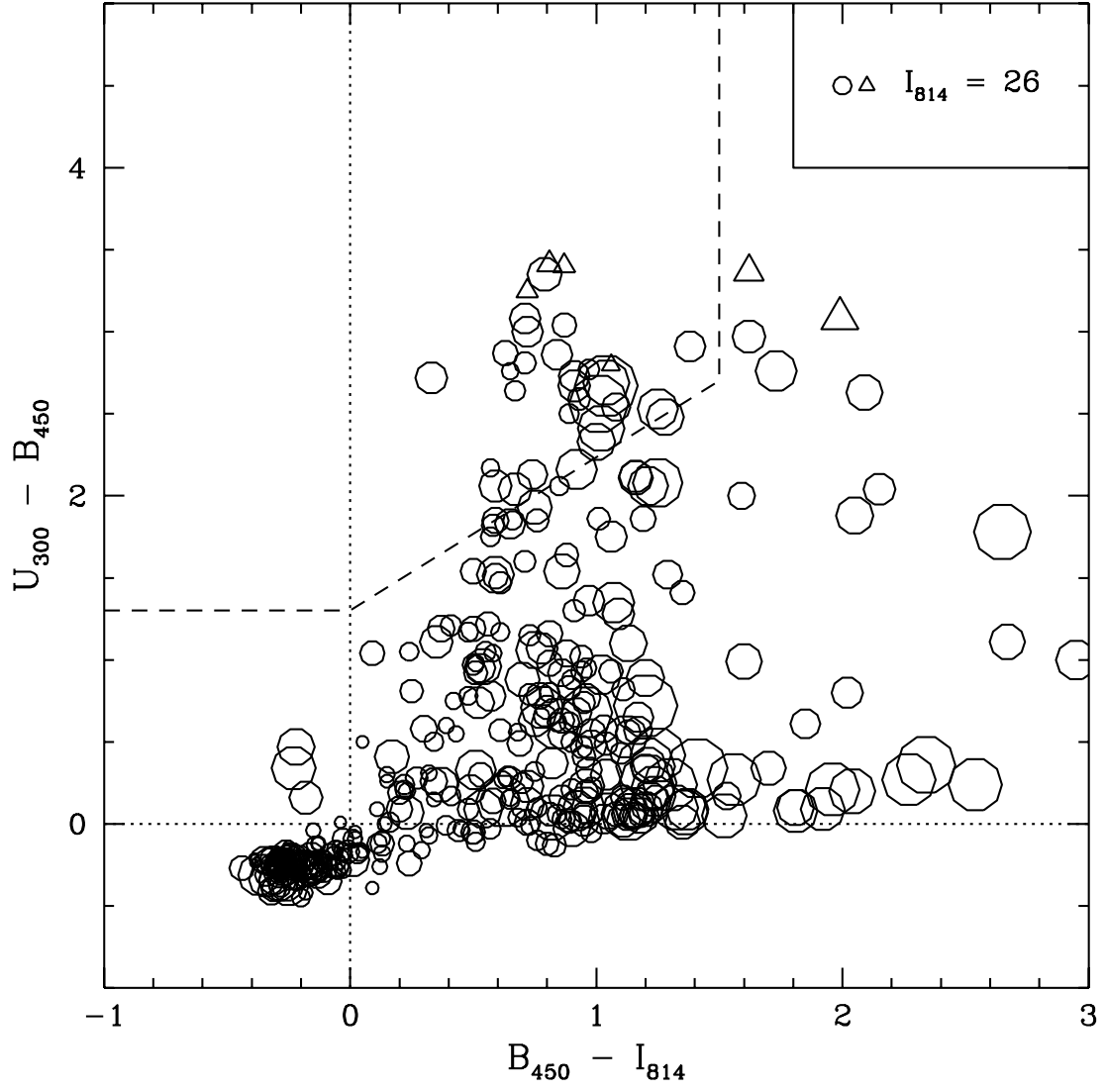


Figure 11b.
 $q_0=0.5$ dwarf-dominated

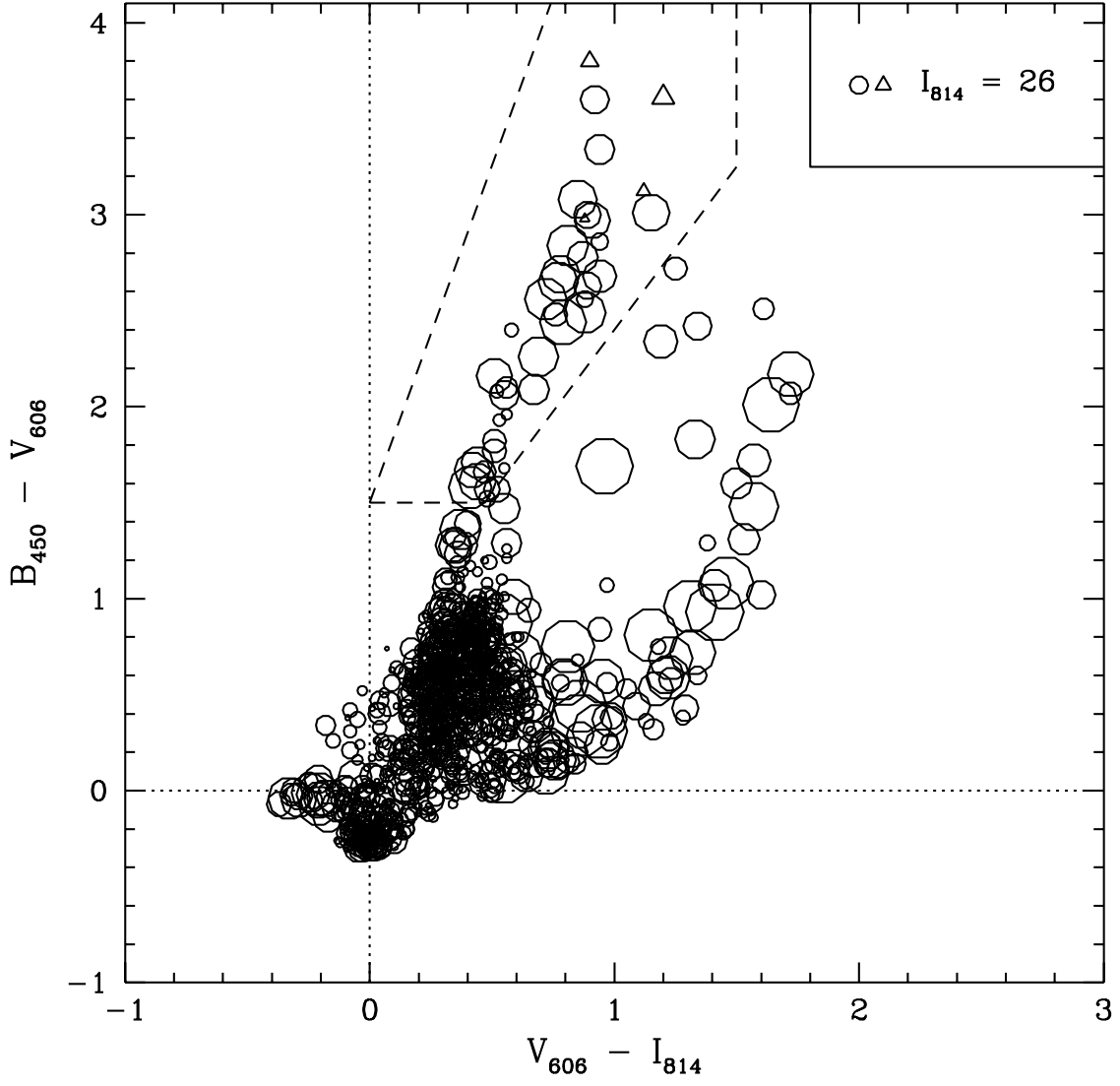


Figure 12a.

$q_0=0.01$

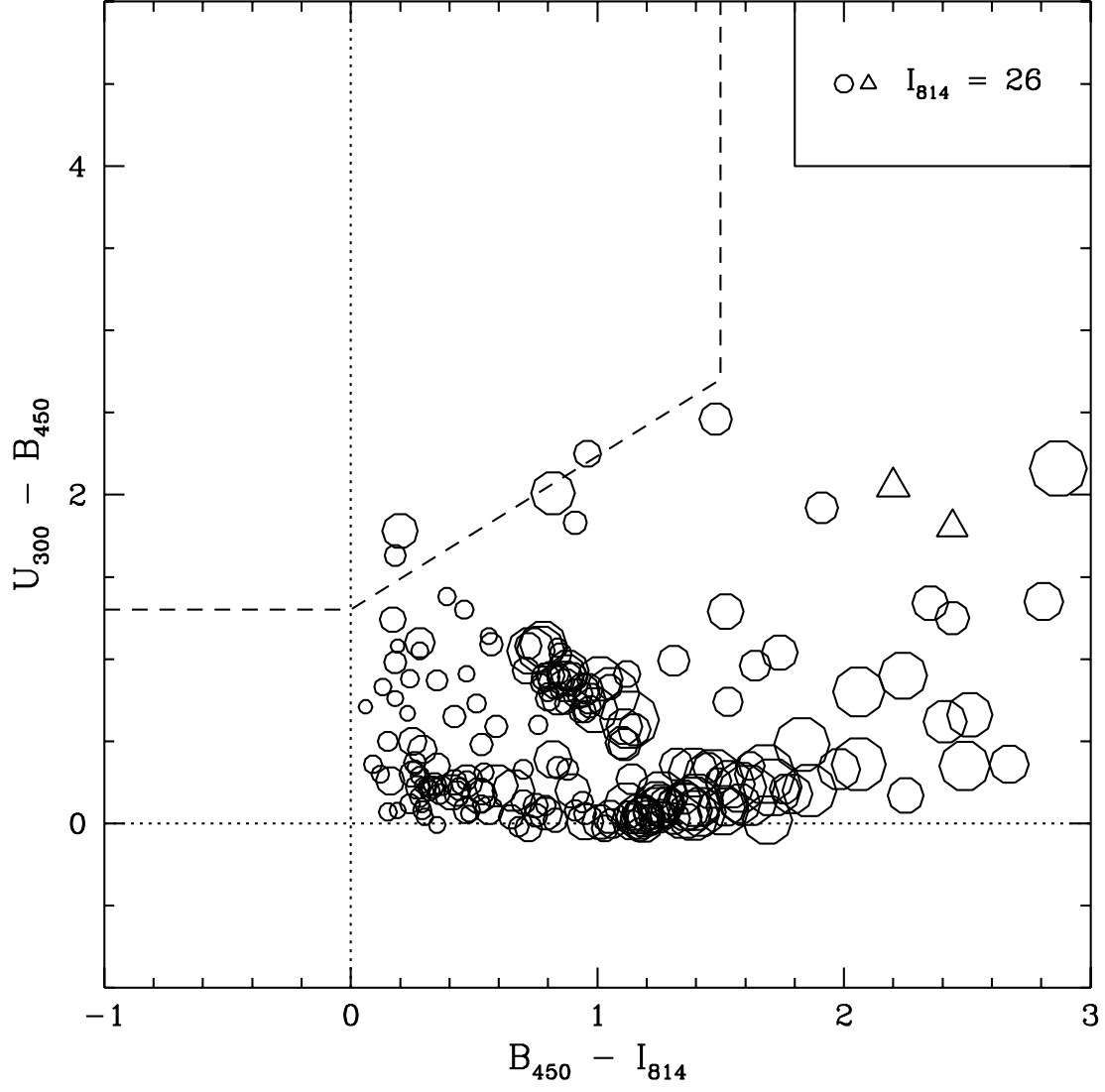
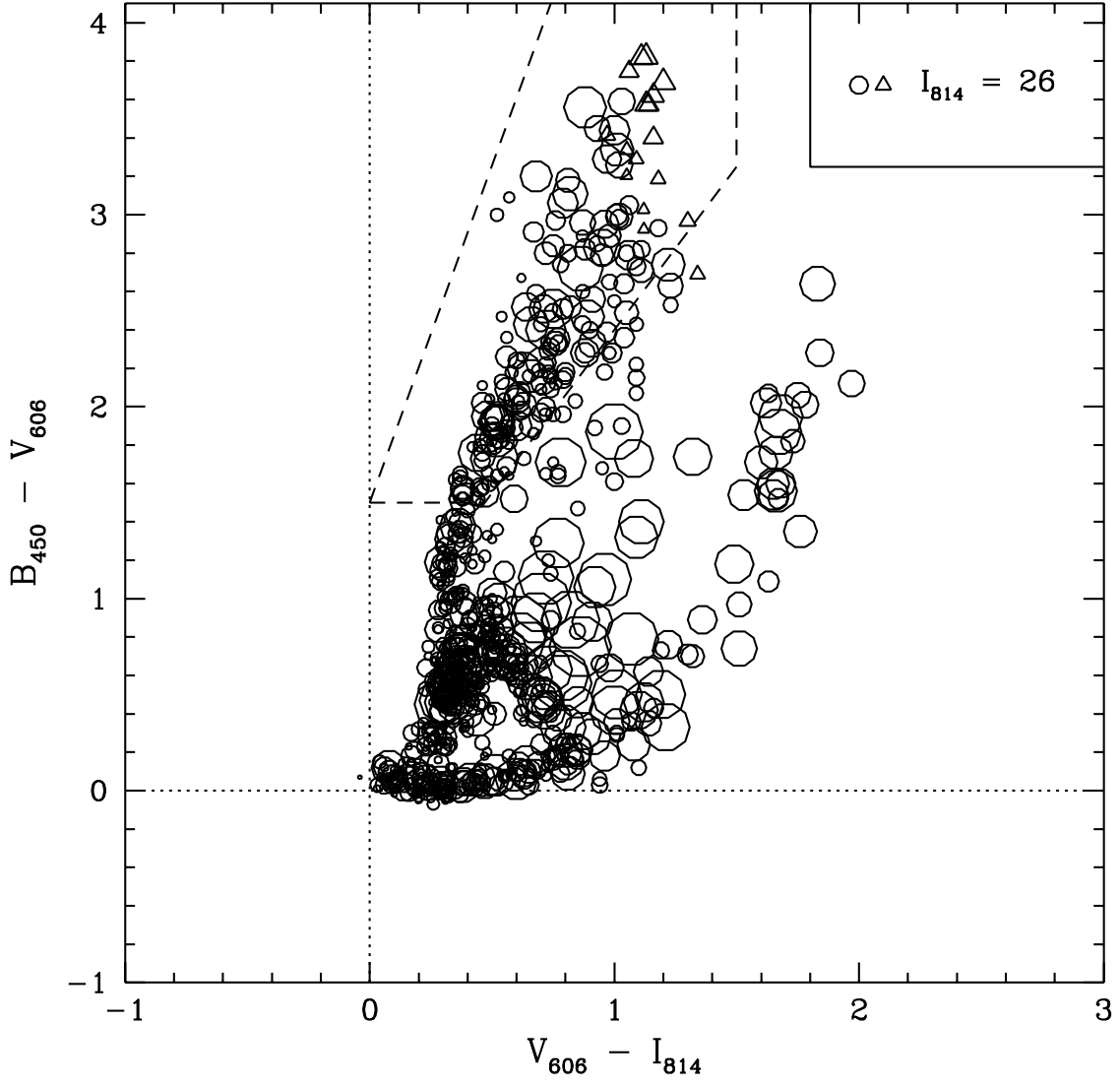


Figure 12b.

$q_0=0.01$



This figure "fig1color.jpg" is available in "jpg" format from:

<http://arxiv.org/ps/astro-ph/9801057v1>

This figure "fig2color.jpg" is available in "jpg" format from:

<http://arxiv.org/ps/astro-ph/9801057v1>

This figure "fig3color.jpg" is available in "jpg" format from:

<http://arxiv.org/ps/astro-ph/9801057v1>